



This is a repository copy of *What triggers a microcrack in printed engineering parts produced by selective laser sintering on the first place?*.

White Rose Research Online URL for this paper:  
<http://eprints.whiterose.ac.uk/92361/>

Version: Accepted Version

---

**Article:**

Ibbett, J., Tafazzolimoghaddam, B., Hernandez Delgadillo, H. et al. (1 more author) (2015) What triggers a microcrack in printed engineering parts produced by selective laser sintering on the first place? *Materials and Design*, 88. 588 - 597. ISSN 0264-1275

<https://doi.org/10.1016/j.matdes.2015.09.026>

---

Article available under the terms of the CC-BY-NC-ND licence  
(<https://creativecommons.org/licenses/by-nc-nd/4.0/>)

**Reuse**

Unless indicated otherwise, fulltext items are protected by copyright with all rights reserved. The copyright exception in section 29 of the Copyright, Designs and Patents Act 1988 allows the making of a single copy solely for the purpose of non-commercial research or private study within the limits of fair dealing. The publisher or other rights-holder may allow further reproduction and re-use of this version - refer to the White Rose Research Online record for this item. Where records identify the publisher as the copyright holder, users can verify any specific terms of use on the publisher's website.

**Takedown**

If you consider content in White Rose Research Online to be in breach of UK law, please notify us by emailing [eprints@whiterose.ac.uk](mailto:eprints@whiterose.ac.uk) including the URL of the record and the reason for the withdrawal request.



[eprints@whiterose.ac.uk](mailto:eprints@whiterose.ac.uk)  
<https://eprints.whiterose.ac.uk/>

## Accepted Manuscript

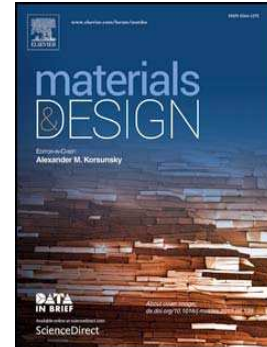
What triggers a microcrack in printed engineering parts produced by selective laser sintering on the first place?

J. Ibbett, B. Tafazzolimoghaddam, H. Hernandez Delgadillo, J.L. Curiel-Sosa

PII: S0264-1275(15)30435-4  
DOI: doi: [10.1016/j.matdes.2015.09.026](https://doi.org/10.1016/j.matdes.2015.09.026)  
Reference: JMADE 596

To appear in:

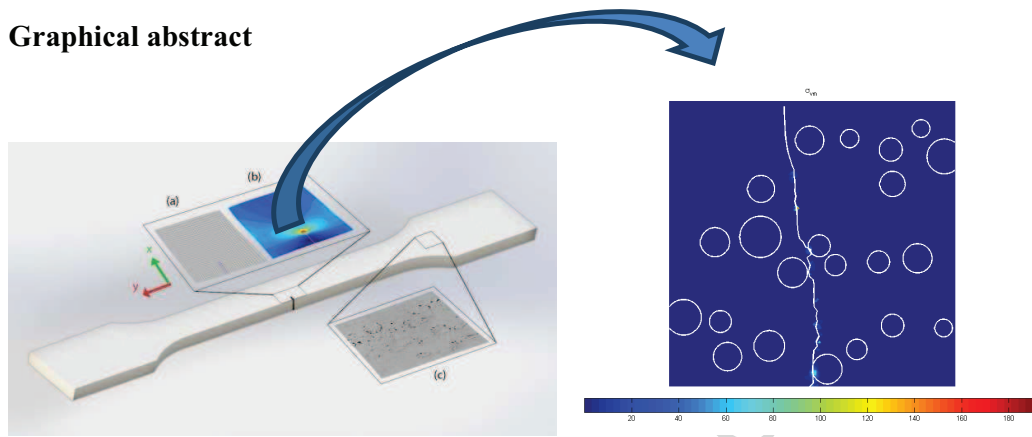
Received date: 13 July 2015  
Revised date: 5 September 2015  
Accepted date: 7 September 2015



Please cite this article as: J. Ibbett, B. Tafazzolimoghaddam, H. Hernandez Delgadillo, J.L. Curiel-Sosa, What triggers a microcrack in printed engineering parts produced by selective laser sintering on the first place?, (2015), doi: [10.1016/j.matdes.2015.09.026](https://doi.org/10.1016/j.matdes.2015.09.026)

This is a PDF file of an unedited manuscript that has been accepted for publication. As a service to our customers we are providing this early version of the manuscript. The manuscript will undergo copyediting, typesetting, and review of the resulting proof before it is published in its final form. Please note that during the production process errors may be discovered which could affect the content, and all legal disclaimers that apply to the journal pertain.

## Graphical abstract



ACCEPTED MANUSCRIPT

# What triggers a microcrack in printed engineering parts produced by selective laser sintering on the first place?

J. Ibbett<sup>a</sup>, B. Tafazzolimoghaddam<sup>a</sup>, H. Hernandez Delgadillo<sup>b</sup>, J.L. Curiel-Sosa<sup>a\*</sup>

<sup>a</sup> *Department of Mechanical Engineering, University of Sheffield, Sir Frederik Mappin, Mappin St, Sheffield S1 3JD, UK.*

<sup>b</sup> *Faculty of Engineering Technology, University of Twente, PO Box 217, 7500 Ae Enschede, The Netherlands*

---

## Abstract

The proximity of un-melted particles within Selective Laser Sintered (SLS) printed engineering parts made of nylon-12 is found as a major triggering effect for cracking and ultimately failure. The numerical investigation, by means of the eXtended Finite Element Method (XFEM), was performed over samples with different arrangements of un-melted particles obtained experimentally. The onset and propagation of microcracks was simulated. This included inherently how the degree of particle melt (DPM) in SLS parts affects and controls both crack initiation and propagation. The results evidenced that a microcrack started invariably between the two closest un-melted particles in all numerical tests performed considering different arrangements of un-melted particles.

*Keywords:* nylon, degree of particle melt, sintering, fracture, particle

---

## 1. Introduction

Since the invention of the technology in the 1980s, the additive manufacturing (AM) industry has progressed a significant distance, going from what was originally an expensive prototyping technique to becoming what can be regarded as a process able to produce end-use parts that can rival the material properties of traditional methods, if the limitations of the technology are properly understood [1]. AM manufacturing processes dis-

---

\*j.curiel-sosa@sheffield.ac.uk (JL Curiel-Sosa). Tel: +44-1142227857. URL: www.jlcurielsosa.org

tinguish themselves from other methods by building parts from CAD (Computer-Aided Design) files separated into layers. These layers are bonded together within the machines in order to produce the parts, differing from the usual subtractive techniques. It is notorious that the material properties of additively manufactured parts vary significantly due to the often inhomogeneous nature of the build parameters used. In addition, the presence of un-melted particles due to incomplete melting introduces instabilities. This means that parts used in a true engineering setting can often fail unexpectedly, often through fracture, and therefore a wider understanding of the performance of printed parts is needed not only with regards to mechanical testing, but also fatigue and fracture behaviour. This can be done experimentally, but often on a microscopic scale where individual particles play a significant role simulation methods can have significant advantages. There are a number of works presenting finite element analyses on laser sintering products, see e.g. [2, 3, 4, 5], however, this is the first time that XFEM [6] is applied to failure analyses of

SLS specimens resulting in new findings on the mechanical behaviour of nylon-12. The main source of failure is attributed to geometric discontinuity or stress concentration. This form of discontinuity usually takes the form of a sharp change of geometry, opening, hole, notch, crack, etc [7]. Modelling and analysis of these discontinuities is meaningful, as it will build on the understanding of their behaviour within Selective Laser Sintered (SLS) parts and will contribute to their enhanced life and performance. The effect to which un-melted particles influence the onset and direction of the propagation of microcracks in SLS printed engineering parts is presented in this study. How the degree of particle melt (DPM) in SLS parts affect and control both crack initiation and propagation is one of the aims of this study. This paper is structured as follows. Firstly, a brief background on additive manufacturing, laser sintering process and properties of nylon-12 is provided. Secondly, tests and results conducted by using the extended finite element method (XFEM) in nylon-12 samples with different arrangements and degrees of particle melt are presented. Finally, discussion of results and concluding remarks are provided.

### *1.1. Additive Manufacture and Laser Sintering Process*

Before the arrival of additive manufacturing, methods of manufacturing were classified as either being ‘forming’ processes or ‘subtractive’ processes, where material was either deformed or removed respectively to shape the final part. Additive manufacturing has provided a new third group where material is instead added, usually in layers, to build up a part [8]. Since the 1980s, when additive manufacture was invented, the industry has been growing and expanding, with new machines, processes and methods being developed every month. Selective Laser Sintering (SLS) [9, 10, 11] is a process which involves starting with an initial powder bed and then generating complex parts by Selective melting the cross section of a part layer by layer. The input of thermal energy via a laser beam provides the means by which the power both melts and consolidates together. The process has

become well established over time as the parts it produces have improved regarding their higher mechanical properties, and reliability between build jobs. The most widely known advantage is that the machine builds directly from a CAD file, so the complexity of the part can be far higher compared to conventional techniques, meaning parts are limited by the process rather than design freedom; this opened the door for many new uses of the technology. Limitations on SLS process include that the final surface finish of the parts is generally poor, where a high amount of post processing is usually required to achieve end-use parts. Thermal variations and build temperatures in the build volume can also cause significant warping and curling of parts, in tandem with incomplete melting introducing unmelted particles, both of which alter the part strength. Although the reliability of the build part properties have improved significantly allowing many more applications, they still pose issues for the technology. In the SLS process, mechanical properties of the produced part are not solely influenced by the base material itself, but also by the process parameters. It is important to breakdown the SLS process and analyse the different parameters which will affect the end properties of the part. Some of the parameters will have a more marked effect on the end mechanical properties than others, and also parameters affect one-another, so the result is a complicated network of interlinking factors. It is outside of the scope of this study consider them all, so in this case, three of the more significant parameters are highlighted next: temperature, degree of particle melt and anisotropy.

- **Feed/Part Bed Temperatures:** The temperature at which the powder feed and part bed is held at influences the end properties significantly.  
The main objective of maintaining part bed temperature is to reduce or eliminate the part distortion during the SLS of nylon-12. Temperatures which are too high can lead to premature melting. Temperatures which are too low can lead to significant deformation and curling of the final parts. Generally, the lower the temperature the lower the density and therefore mechanical properties [12]. The Part Bed Temperature,  $T_b$  is the temperature at which the powder is held within the central part cylinder or bed, in which the part is built. This temperature is usually reached via a *preheat* where the  $T_b$  value is obtained before any of the laser parts move. The Powder Feed Temperature  $T_f$  is the temperature at which the powder in the powder supply is held before it is dispensed across the powder bed. The rheology of the powder as it is applied is strongly affected by this value. In an ideal scenario, the temperature of the powder is as close to the melting temperature as possible without the powder prematurely consolidating or thermally degrading. This reduces the thermal gradient and expansion due to laser heating resulting in parts with lower roughness and better properties [13]. When establishing the simulations, it is assumed that any parts are built under this ideal condition.
- **Degree of Particle Melt (DPM):** The Degree of Particle Melt (DPM) conveys the idea that during the sintering process many particles within a SLS printed part may not

have achieved the fully melted state, and, hence, have un-melted cores. These regions arise where insufficient energy has been input to the powder in order to fully melt the particles. The amount of energy input to the material will determine the proportion of the powder which is fully melted, so defining a universal energy density based on the machine parameters is necessary. This has been known as the Andrew Number in Equation 1 [14] which defines energy density as follows:

$$\text{Andrew Number} = \text{Energy Density} = \frac{\text{Fill Laser Power}}{\text{Scan speed} \times \text{Scan Spacing}} \quad (1)$$

1. Fill Laser power determines to what degree the laser will heat the powder (measured in W), where it will melt and flow allowing coalescence to occur.

$$\text{Fill laser power} = P = \frac{BS \times \rho \times D_b \times C \times [(T_m - T_b) + L_f]}{1 - R} \quad (2)$$

where  $BS$  is the laser beam speed,  $D_b$  denotes diameter of the laser beam,  $C$  is the specific heat,  $T_m$  denotes the powder melting temperature,  $T_b$  is the part bed temperature,  $L_f$  is the latent melting heat, and  $R$  is the reflectivity

2. Scan speed determines the speed at which the laser travels, influencing the fill laser power and building time
3. Scan Spacing refers to how close together each scanned path is, and should not exceed the diameter of the beam itself.

The higher the energy density, the higher the chance the larger particles in the powder will melt, which decreases the chance of un-melted particles. It was concluded by [15] that the varying energy input into the SLS process directly affects the completeness of melting within the part. If a Differential Scanning Calorimetry (DSC) test is performed on an SLS part, two distinct melt peaks are observed which relate to the presence of the both un-melted and crystallised regions around un-melted particles. The relationship between these two proportions is what is used to define the DPM which strongly affects the mechanical properties and thus usefulness of a part.

From the DSC scan a percentage crystallinity can be calculated based on the relation between the two peaks and the temperature at which they occurred. This represents the ratio between the un-melted cores and melted/re-crystallised material. Based on the research by [16], the crystallinity of a fully melted part and powder itself was found to be 25% and 47% respectively. Further to this, from the DSC data the Melted and Crystallised Material (MCM) crystallinity can be calculated along with the core crystallinity defined as being  $[1-\%MCM]$ , the DPM can be calculated using Equation 3. Having calculated the DPM of the part, it is then possible to perform a study to relate the DPM to the overall mechanical properties. By investigating how

the tensile strength is affected by the energy input (and therefore DPM) the behaviour trends can be observed [17]. There is an optimal point of DPM with regards to the value of tensile strength. As the DPM increases, the number of un-melted cores decreases, where the material goes from being a 'double phase' structure with both melted and un-melted Nylon-12 to a 'single phase' structure where the material is fully melted. During this increase in DPM the tensile strength also increases, but beyond the optimal DPM, the tensile strength then drops. This sudden tipping point is not easily explained but shows that once melting is complete the trends become different, meaning that the structure can be treated as a new material. From these trends, it is clear that the degree of DPM and therefore number and structure of un-melted particles plays a crucial role in determining part strength. When establishing the simulation conditions, the DPM is certainly the most crucial factor, where DPM directly determines the number of un-melted particles and thus fracture behaviour.

$$\text{DPM (\% MCM)} = \frac{\text{Total Crystallinity} - \text{Core Crystallinity}}{\text{MCM Crystallinity} - \text{Core Crystallinity}} \quad (3)$$

- **Part Orientation and Anisotropy:** A factor which is almost exclusive to Additive Manufacture is the dependence of the part properties on the orientation and placement of parts within the build volume, meaning they exhibit anisotropy. The manufacturing process builds up parts layer by layer, so the bonding between layers, warping/curling effects which come into play and the interaction between layers impact heavily on the resulting mechanical strength. A variety of studies have been performed investigating the anisotropy of SLS parts, where [18] took standard process parameters and built tensile bars in the x,y and z orientations. The samples were subjected to flexural and compressive tests to determine the degree of anisotropy [19] printed nylon PA12 tensile bars again across the x,y and z directions, but this time using both new and aged powder. The parts were tested to failure on a uniaxial tension test machine. Parts built in the z-orientation are significantly weaker than in other directions, which is due to the inter-layer bonding as they are built up. The process of layer addition is the driving factor causing the anisotropy, which may seem trivial but it often limits the process. For example, a part which has been printed in the z-direction may exhibit significantly different fracture behaviour due to the contrast between inter-layer bonding regimes. In order to simplify this study, it was assumed that all parts investigated were printed in the same direction, thus factoring out the anisotropy.

Although it is possible to process almost any material with the SLS process (as long as it is available as a powder), ranging from metals to ceramics [20], in this study only Nylon-12 is being investigated. A benefit of this is that Nylon-12 is the most widely processed and applied material with SLS, but polymers in general including other semi-crystalline and

amorphous polymers are also widely dealt with [21]. The good mechanical properties of the sintered Nylon-12 makes it excellent for end use applications. The reproducibility of the mechanical properties however poses an issue where the currently unreliable production of end-use parts limits the use of AM in industry. A better understanding of the material and its behaviour when it undergoes the micro-structural changes during sintering is needed, especially with regards to fracture. This includes the presence of un-melted particles within the structure.

### 1.2. Nylon-12 Properties and Sintered Micro-structure

Having many different manufacturers of polymers, there are a variety of Nylon-12 available. Two of the largest companies involved in the selling of polymer powder are EOS and 3D Systems. In general, the material properties do not vary extensively between powders before they have been sintered but it is important to recognise the range available and the impact that it can have on end part properties. The material properties of Nylon-12 from EOS and 3D systems are shown in Table 1

	3D Systems	EOS
Tensile Strength (MPa)	44	45
Tensile Modulus (MPa)	1600	1700
Tensile Elongation at Break (%)	9	20
Part Melting Point (°C)	184	184
Particle Size, average ( $\mu\text{m}$ )	58	58
Particle Size, range 90% ( $\mu\text{m}$ )	25-92	Not Available
Part Moisture Absorption, 23°C (%)	0.41	0.52

Table 1: Manufacturers published material properties for SLS Nylon-12 from [22] and [23]

Based on the process parameters investigated thus far it is clear that the number of variables which affect the end properties of the part is many, so an element of simplification is necessary. During the process of sintering, a number of physical processes occur to take the particle distribution and consolidate them with the input of heat energy and melting to form a material cross section [24]. The degree of sintering and properties of the end product are strongly dependant on the SLS machine parameters discussed [25]. It is also necessary to note that the excess powder to be recycled after each process is completed thermally degrades and leads to subsequent lower mechanical properties when it is used again. Therefore, for the purpose of this project all powder is assumed to be so-called 'virgin' unused powder. To fully define the material in the *in-house code*, the Young's modulus and Poisson's ratio are needed for both the sintered material and un-melted inclusions. A range of studies have been researched documenting the varying material properties. [26] looked into how the Young's Modulus changed with a variation in energy density for printed

parts orientated at either  $0^\circ$  or  $90^\circ$ . It was found that the Young's modulus varies quite significantly with the given variables, ranging from 600-1100MPa as energy density changed from 0.005-0.03J/mm<sup>2</sup>, where also in general the parts orientated at  $0^\circ$  had a higher modulus value. [27] conducted experiments where the machine parameters remained constant but the section thickness and part orientation were varied. The range of Young's Modulus values again varied a lot, from 1200-4000MPa across the whole range of orientations and part dimensions. [28] measured the change in compressive properties of laser sintered and injection moulded nylon-12 parts both experimentally and computationally. The variation of properties with machine parameters was not investigated, but the average compressive Young's modulus value was found to be 820MPa. [29] fabricated a variety of test bars with varying energy inputs, scan speeds, scan spacings, layer thickness and orientations. The article states that Young's Modulus increases sharply up to an energy input of 0.12J/mm<sup>3</sup> but reports little change after that. This would be due to the value of DPM approaching 100%. The value of Young's modulus varies between 1700-2000MPa. It is clear that the Young's Modulus of the final part can be controlled and selected by the user by changing process parameters. Considering all of the articles discussed, it would seem sensible to choose a Young's modulus value of 1800MPa to be used, a rough average of all the values. The value of Young's modulus for the un-melted particle cores must also be determined. For the simulations, it is assumed feasible for the value of Young's modulus for the un-melted cores to be ten percent higher than the regular material [17].

## 2. eXtended Finite Element Method *in-house code*

The eXtended Finite Element Method [6, 30] (XFEM) is regarded as an effective numerical methodology for fracture assessment in materials. The tests presented herein have been obtained with an XFEM implemented in an in-house code. The *in-house code* used was originally developed by Matthew Pais at the University of Florida [31], originally a collection of MATLAB subroutines released as open-source to increase understanding of the XFEM method in general [31]. It has been modified in order to suit the needs of this study, where edits are made in order to be able to collect data and figures after each iteration <sup>1</sup>, but the majority has remained unchanged. The code is relatively easy to modify, having a single MATLAB input function to change the variables. This code is particularly convenient to model dynamic cracks as eliminates the need for re-meshing [32] when the fracture propagates [33]. Applications of XFEM proving its convenience in the fracture mechanics field are found on the literature. For instance, in the work by [34], XFEM was applied in modelling the delamination in mode I of hybrid composite material.[35, 36] used XFEM to analyse crack initiation and propagation in a composite cruciform specimen subjected to

---

<sup>1</sup>Henceforth, iterations are referred to numerical iterations of the XFEM solver of the in-house code

quasi-static biaxial loading. XFEM allowed the modelling of imperfections in the geometry, and meant the domain of study could be analysed without the need to know *a priori* the crack path. XFEM is mesh-independent for the simulations performed (below) even at relatively coarse meshes, saving on computational time.

### 2.1. Extended Finite Element Method Features

The extended finite element method (XFEM) [6, 30] has arisen from the need to simulate cracks as they propagate through a continuum amongst other problems. It is a relatively new method which builds on the Finite Element Method (FEM) [37]. In particular, an explicit solver [38, 39] for FEM is used herein. XFEM is a FEM in which enrichment functions –interpolation– are added to the standard approximation. Note that a multiscale FE approach [40] is not used herein. The concept of partition of unity is used to ‘enrich’ the classical FEM mesh in order to cater for the added complexities such as inclusions or discontinuous crack fields. The discontinuities in XFEM are arbitrarily aligned within the mesh, and are represented by means of enrichment functions [41]. The XFEM features used for this investigation are provided below in some detail. For a didactic overview of XFEM the interested reader is referred to [42, 43]. The enrichment is basically an interpolation based on additional degrees of freedom to account for special features as crack discontinuity [44], see Equation 4, where  $x$  is a point within a FEM model and there is a discontinuity which is in a domain discretised into  $n$  number of finite elements.

$$u^h(\mathbf{x}) = u^{std} + u^{enr} = \sum_{j=1}^n N_j(\mathbf{x}) \cdot u_j + \sum_{\mathbb{B} \in \Gamma_{enr}} \sum_{k=1}^m \psi_k(\mathbf{x}) \cdot N^{\mathbb{B}}(\mathbf{x}) \cdot a_k^{\mathbb{B}} \quad (4)$$

where  $N_j$  and  $N^{\mathbb{B}}$  are shape functions for normal and enriched nodes, respectively.  $u^{std}$  are displacements of standard degrees of freedom,  $u^{enr}$  displacement associated to additional degrees of freedom, e.g. the jump occasioned by a crack in the displacement field,  $a_k$  are the added degrees of freedom and  $\psi$  is a special function to effectively computed the discontinuity associated to a crack or the asymptotic field ahead of the crack tip as explained in the next sections.

#### 2.1.1. Heaviside Enrichment

In order to fully define the crack in the domain, two different enrichment functions are needed, one to model sections which have been completely cut by the crack, and another to model the crack tip as it propagates through the material. The former is called the Heaviside enrichment function and takes the following form:

$$\psi(x) = \begin{cases} +1 & \text{if } x \geq 0 \text{ (above crack);} \\ -1 & \text{if } x < 0 \text{ (below crack).} \end{cases} \quad (5)$$

This form represents a discontinuity or 'jump function' which gives a similar stress and strain fields on both sides of the crack. The method works on adding further independent, virtual degrees of freedom to the elements around the crack.

### 2.1.2. Tip Enrichment

The tip of the crack surrounding zone often requires an additional enrichment to represent the special asymptotic field and, hence, additional degrees of freedom are required. This is performed through the following set of functions:

$$\psi_{\alpha}(x)_{\alpha=1-4} = \left[ \sqrt{r} \sin \frac{\theta}{2}, \sqrt{r} \cos \frac{\theta}{2}, \sqrt{r} \sin \theta \cos \frac{\theta}{2}, \sqrt{r} \sin \theta \cos \frac{\theta}{2} \right] \quad (6)$$

where  $r$  and  $\theta$  are the polar coordinates in the local crack-tip coordinate system.

### 2.1.3. Inclusion Enrichment

In our particular problem, an additional enrichment is needed to define how un-melted particles interfaces are modelled. An enrichment function was originally proposed by [45] which took the form in Equation 7, where  $\zeta_I$  represents the nodal level set [46, 47] values for the material interface level set equation.

$$\psi(x) = \left| \sum_I N_I(x) \zeta_I \right| \quad (7)$$

where  $\zeta_I$  are additional degrees of freedom and  $N_I(x)$  are the shape functions. It was however found, that the formula had problems when blending the enriched and non-enriched zones. This problem was solved by [48] afterwards using an absolute enrichment value, which is shown in Equation 8. The formula was proven to have optimal convergence [49].

$$\psi(x) = \sum_I N_I(x) |\zeta_I| - \left| \sum_I N_I(x) \zeta_I \right| \quad (8)$$

## 3. Results

### 3.1. Test 1

The aim of test one is to investigate the effect of the location and properties of particle inclusions within the domain the crack behaviour, including the propagation direction,

angle and magnitude. In addition, it was to investigate the effect of varying stiffness of the un-melted particle inclusion. A plane strain state is applied with increasing loading to fracture further the specimen and allowing crack progression. The nylon-12 material properties have been defined above. Figure 1 shows how the mesh is defined with the inclusion representing an un-melted particle. Henceforth, inclusion is used indistinctly as synonymous of un-melted particle. The test involves changing the location of the inclusion and iterating to see how it affects crack behaviour. All length units are given respect to the size of the un-melted particle. Thus, the sample dimensions are set to Height = 6, i.e. six times the size of the inclusion diameter, Width = 3, length of element side (LElem) = 1/20, i.e. 1/20 of the inclusion diameter, and initial notch length = 0.75. Ten iterations were performed with a crack propagation constant of 0.1. In Figures 2, 3 and 4, the results of those tests can be seen. It is clear that the crack angle and direction is affected by increased proximity of the particle to the initial notch, where the magnitude by which the crack is angled away increases as the particle becomes closer.

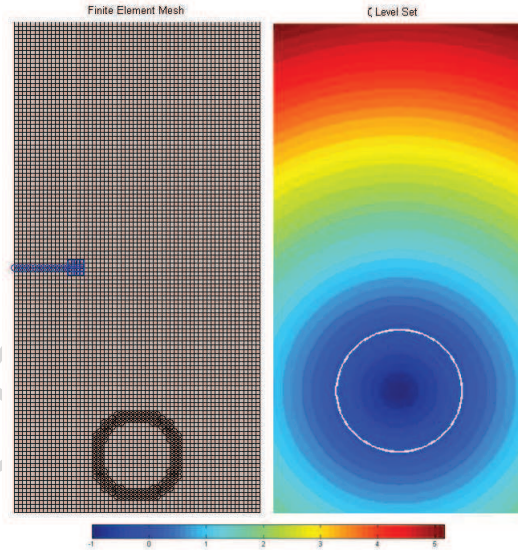


Figure 1: Test 1: details of finite elements mesh and enrichment on initial notch and interface (lhs). Level sets used within the XFEM simulation (rhs). For details of level sets description refer to [46, 47]

### 3.2. Test 2

The second test investigated the way in which the proximity of two particles affects crack behaviour. An offset edge crack was set up similar to that in test one. Two particle inclusions are added with a small gap or 'bottle neck' between them in order to see the effect of the concentrated area between them. The question was whether when particles are in close proximity to one another they act as stress concentrators and therefore will cause

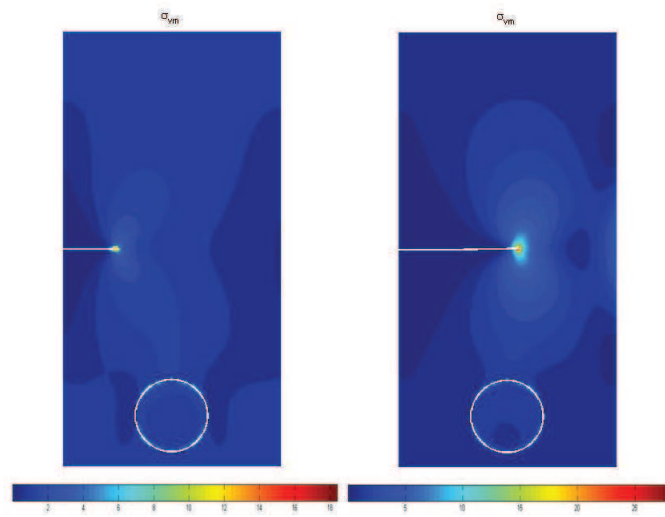


Figure 2: Test 1.1: farthest –to crack– un-melted particle (centre at [1.5,0.7] and radius of [0.5]). Figure depicting Von-Mises stress field (MPa) and crack evolution: initial (lhs) and final crack length (rhs)

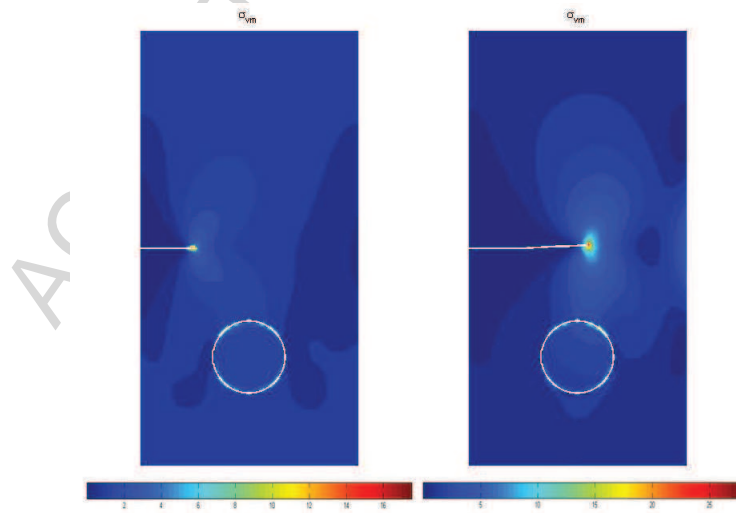


Figure 3: Test 1.2: middle un-melted particle (centre at [1.5,1.5] and radius of [0.5]). Figure depicting Von-Mises stress field (MPa) and crack evolution: initial (lhs) and final crack length (rhs)

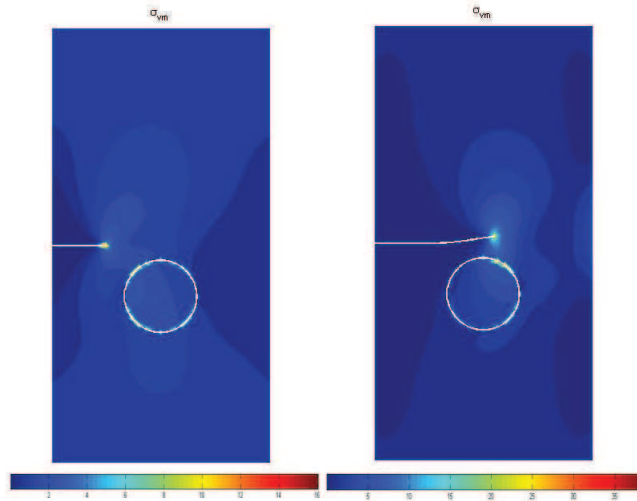


Figure 4: Test 1.3: un-melted particle (centre at  $[1.5, 2.3]$  and radius of  $[0.5]$ ). Figure depicting Von-Mises stress field (MPa) and crack evolution: initial (lhs) and final crack length (rhs). The crack angle and direction is affected by increased proximity of the particle, where the magnitude by which the crack is angled away increases as the particle has become closer than in experiments 1.1 and 1.2

the crack to steer towards them. The sample and finite element mesh was set up with Height = 8, Width = 4 and LElem = 1/40 (all units respect to the inclusion diameters). The increased number of elements was to allow for the crack propagation and stress distributions between the two particles to be seen more clearly. 40 Iterations were performed with a crack iteration constant of 0.05, where the reduced crack iteration constant allowed for finer observation of the crack. The inclusion centre locations are set with coordinates  $[1, 3.4]$  and  $[1, 4.6]$  where both un-melted particles have a radius of  $[0.55]$ . The un-melted particles are assumed ten percent stiffer [17]. It can be seen from Figure 5 that the crack has steered towards the gap between the two particles and passed through the other side. There are red regions between the two particles which indicate that at those points the levels of stress are higher.

### 3.3. Tests 3 and 4

Tests 3 and 4 analyse situations which are closer to a real case. The geometrical configuration or un-melted particles arrangement have been reproduced from [50].

Circles stand for the level set modelling [46, 47] the interface zone between un-melted particles and the surrounding continuum that has been melted. The sizes and distribution comes from experimentally obtained configurations by [50]. The general aim of the experiments are to have simulations with parameters based on the previous experiments but where the

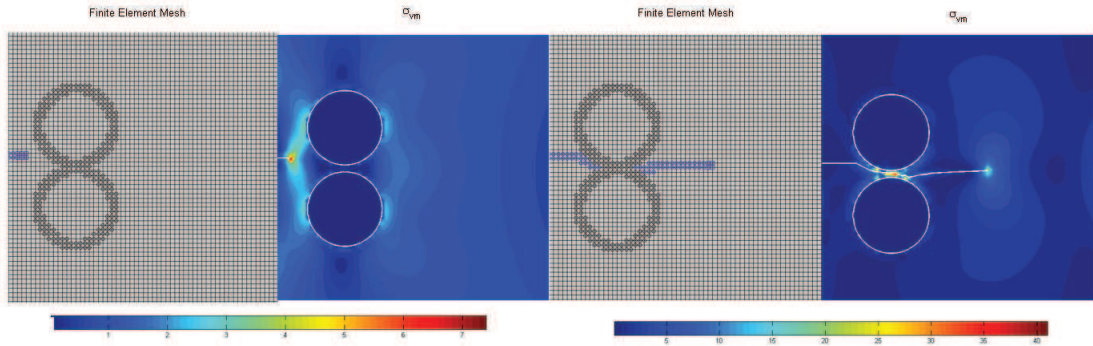


Figure 5: The two figures on the LHS depict the mesh and Von Mises stress plots for the initial crack. The two RHS figures show the final length of the crack in the simulation.

inclusions added represent the cross section of a real SLS printed part. The process parameters used to print this part are shown in Table 2 corresponding to the configuration depicted in Figure 6.



Figure 6: Test 3 simulation depicting the onset of crack between the two closest un-melted particles. Contours represent the Von-Mises stress field (max. displayed in red).

Part bed set-point ( $^{\circ}\text{C}$ )	Scan Speed (mm/s)	Scan spacing (mm)	Laser power (W)
149	5000	0.15	11

Table 2: Build parameters used to produce the SLS part in test 3 [50]

Test four mirrors the same simulation parameters of test 3 except for the number, location and size of un-melted particles. The result of test 4 is depicted in Figure 7. The cross section for this part was reproduced from [50], where optical microscope images of micro-toned specimens were taken from a build where the properties are shown in Table 3. In order to

be able to compare tests 3 and 4, the simulation settings remained the same between the two. The load was increased gradually up to complete failure, the magnitude was variable but the values of the Von-Mises stress can provide detail of the stress undertaken by some of the samples. The crack initiated in both experiments 3 and 4 at the point where the proximity between particles is closest, where the stresses are reaching peak values.

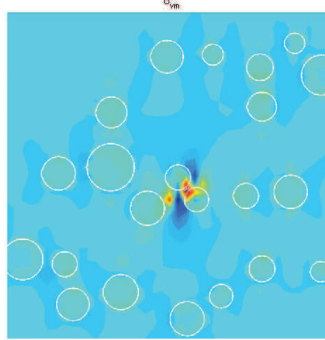


Figure 7: Test 4 simulation showing initiation of crack between the two closest un-melted particles. Contours represent the Von-Mises stress field (max. displayed in red).

Part bed set-point ( $^{\circ}\text{C}$ )	Scan Speed(mm/s)	Scan spacing (mm)	Laser power (W)
148	6300	0.15	9.5

Table 3: Build parameters used to produce the SLS part in test 4 [50]

### 3.3.1. Calculating the Percentage of Crystallinity

Based on Figures 6 and 7 and Equation 3, the value of % Crystallinity can be calculated for both tests 3 and 4 specimens. If DSC experiments were completed for the samples, the DPM could then be calculated from the relative peak sizes, however for the purpose of this study the value of % crystallinity gives a good idea of the relative completeness of melting in the samples. The results of these are shown in Table 4.

### 3.3.2. Remarks: experiments 3 and 4

Figure 8 shows the propagation of a single crack through the material, where 25 iterations were completed before one end of the crack reached the edge of the domain, thus resulting in part failure. It shows the iterations where significant change in the crack path occurred. It can be seen that the direction of crack propagation is influenced by the presence of

Test 1	Particle Core	MCM	Domain	Test 2	Particle Core	MCM	Domain
Areas	11.97	88.03	100	Areas	9.917	90.08	100
% of Domain	0.1197	0.8802		% of Domain	0.1549	0.8451	
× Crystallinity	5.628	22.00		× Crystallinity	7.282	21.12	
% Crystallinity	27.634			% Crystallinity	28.409		

Table 4: Calculation of % crystallinity for tests 3 and 4.

the particles, where the severity of curving would not appear to be that high. The initial change in crack path curvature is far higher compared to subsequent iterations. Figure 9 shows the results of test 4, where again the crack can be seen in the collection of figures as it grows through the material. 27 iterations were completed before the crack reached the edge of the domain and thus stopped. It can be seen that the crack has passed through one of the particle inclusions at the bottom of the domain, where the crack path veered sharply as it entered. The crack curved significantly at the start where the size and proximity of the particles is high. It can also be seen that the path remained relatively straight in the upper region where the density of particles is low.

#### 4. Discussion of results

Three test programs were conducted to investigate the effect to which un-melted particles influence the behaviour of the propagation of microcracks in SLS printed engineering parts. In test one, it is proven that the level of proximity of an un-melted particle strongly affects crack direction. The degree of change in the angle is easily observed from the figures and seen to be of significance. The reason why the crack bends away from the un-melted particle is a result of the altered fracture toughness conditions around the crack tip due to particle proximity. The stresses around the un-melted particle interface itself are also increased, meaning the bond between the medium itself and particle is affected by crack proximity. Test two affirms that a 'bottle neck' of two particles together results in the crack 'steering' toward that location, where it can be clearly seen that the proximity leads in an extreme concentration and increase of the stresses. This would certainly result in extreme damage of the material in most cases. Regarding tests 3 and 4, it was observed that in the initial state, the presence of particles leads to extreme concentrated stress around the crack. The aim was to make a connection between the arrangement of particles and crack behaviour. Firstly, the elevated stress present at the particle/material boundary is increased with particle size, which is caused by shear stress interaction at the interface and leads to increased damage. The levels of crystallinity of both experiments were relatively low at  $\simeq 27\text{-}28\%$ , where test four exhibited fewer, larger un-melted particles. The former required fewer iterations for the crack to propagate to the edge of the domain, meaning the part failed sooner. It is assumed that the higher laser power and lower scan speed were

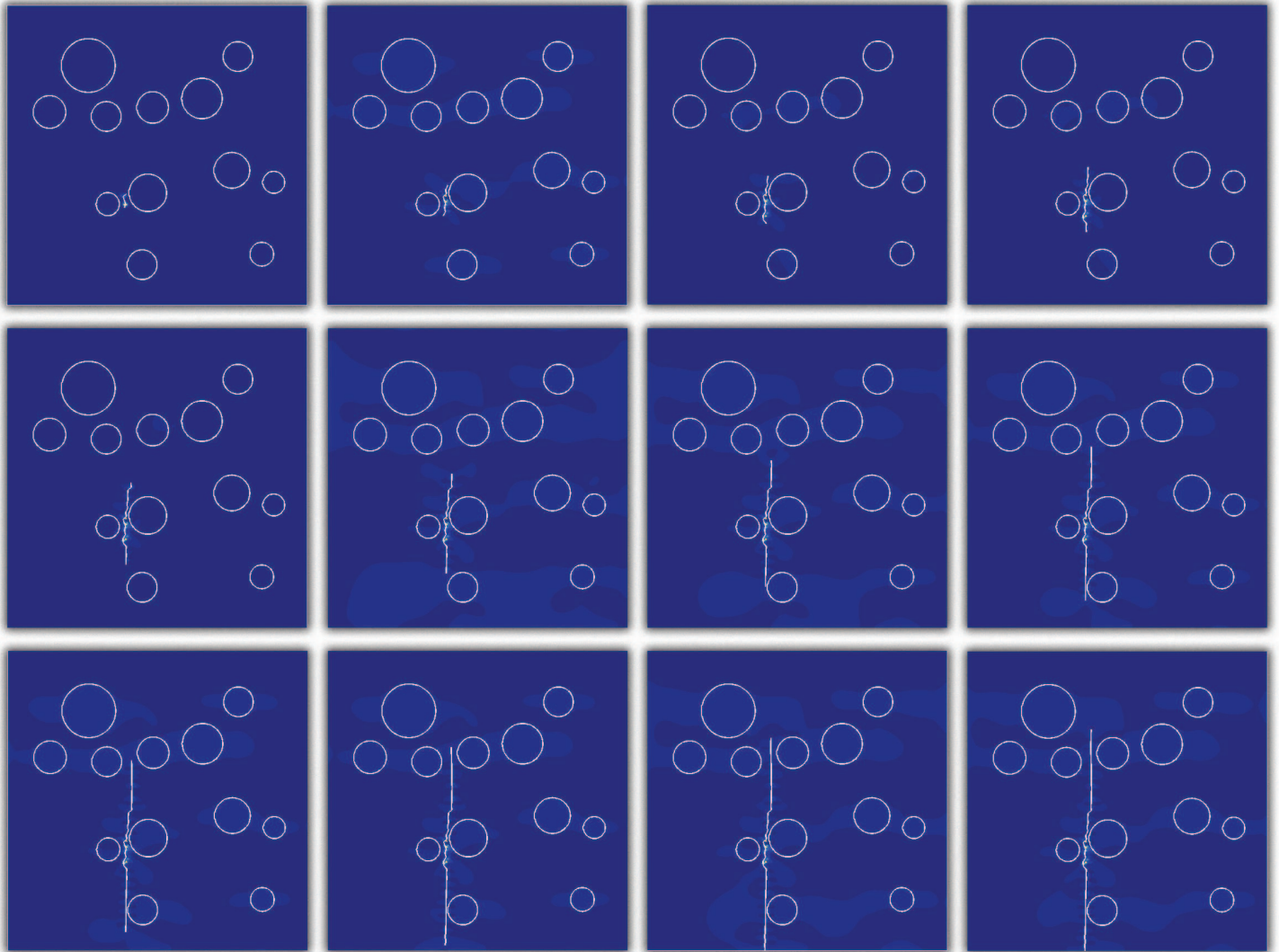


Figure 8: 12 Individual figures showing the crack growth path and Von Mises stress distribution throughout the iterations for test 4.

The curves of the crack have progressed in the simulation with the extended Finite Element Method using level sets [46, 47], i.e. once the criterion of crack propagation is satisfied the elements are partitioned.

the cause of the earlier failure, despite that the sample had a lower value of crystallinity. From this it can be postulated that the size and location of inclusions impacts of fracture behaviour more than the number. Test 4 shows that the higher the initial proximity of

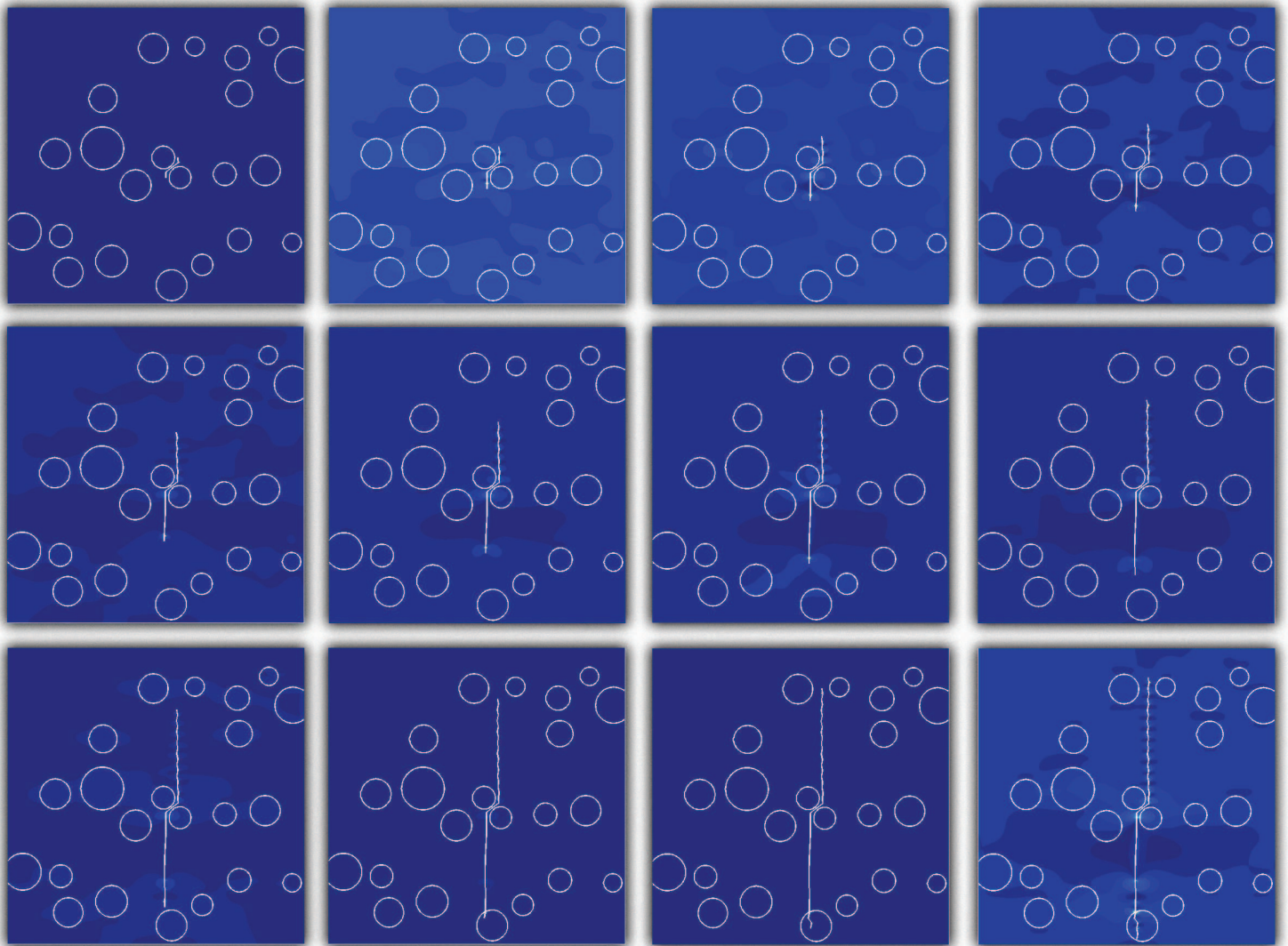


Figure 9: 12 Individual figures showing the crack growth path and Von Mises stress distribution throughout the iterations for test 4

particles causing the crack, the more sharply the initial crack path will change. In addition, the higher number of smaller particles lead to the crack penetrating an un-melted particle.

## 5. Conclusion

Simulation results pointed out that the presence of un-melted particles within the sintered Nylon-12 material of a SLS part has a significant effect on its behaviour under loading with respect to the growth of dynamic cracks. The way in which un-melted particles can affect crack growth was investigated, where it was observed that not only the location, but size and number of un-melted particles lead to drastic changes in crack path and thus fracture behaviour. On view of the performed tests, the role of un-melted particles can be summarised as follows:

1. Absence of particles entirely, or lack of close proximity leads to little or no effect on the crack direction.
2. The closer a particle is to a crack, the more strongly its direction is affected.
3. The presence of a 'bottle neck' of two particles leads to the most significant change in crack behaviour.
4. Initiation of a crack on the first place occurs between the two closest un-melted particles.

Based on this, it can be concluded that wherever possible the optimum level of DPM in a part should be strived for as ultimately un-melted particles proximity lead to premature part failure. As this is often unobtainable, then, a printed part with smaller and more sparsely arranged particles has a more favourable set of fracture properties. Therefore, an initial smaller size of particles and as sparsely distributed as possible is the driving factor for more resistant SLS printed parts.

## References

- [1] B.V. Hooreweder, D. Moens, R. Boonen, J-P. Kruth, and P. Sas. On the difference in material structure and fatigue properties of nylon specimens produced by injection molding and selective laser sintering. *Polymer Testing* 32, pages 972–981, 2013.
- [2] J. Munguia, S. Akande, and K.W. Dalgarno. Compliant flexural behaviour in laser sintered nylon structures: Experimental test and finite element analysis - correlation. *Materials and Design*, 54:652–659, 2014.
- [3] S.P. Soe and D.R. Evers. Fea support structure generation for the additive manufacture of castform™ polystyrene patterns. *Polymer Testing*, 33(1):187–197, 2014.
- [4] C. Deng, M. Liu, and P. Molian. Nanodiamond powder compaction via laser shock-waves: Experiments and finite element analysis. *Powder Technology*, 239:36–46, 2013.

- [5] A. Cerardi, M. Caneri, R. Meneghello, G. Concheri, and M. Ricotta. Mechanical characterization of polyamide cellular structures fabricated using selective laser sintering technologies. *Materials and Design*, 46:910–915, 2013.
- [6] T. Belytschko and T. Black. Elastic crack growth in finite elements with minimal remeshing. *International Journal for Numerical Methods in Engineering*, 45(5):601–620, 1999.
- [7] S. Mohammadi. *Extended Finite Element Method for Fracture Analysis of Structures*. Blackwell Publishing, 2008.
- [8] J. P. Kruth. Material in-process manufacturing by rapid prototyping techniques. *Annals of the CIRP*, 40, 1991.
- [9] S. Kenzari, D. Bonina, J.M. Dubois, and V. Fournée. Quasicrystal-polymer composites for selective laser sintering technology. *Materials and Design*, 35:691–695, 2012.
- [10] B. Zhang, H. Liao, and C. Coddet. Effects of processing parameters on properties of selective laser melting mg-9 *Materials and Design*, 34:753–758, 2012.
- [11] K.B. Hazlehurst, C.J. Wang, and M. Stanford. An investigation into the flexural characteristics of functionally graded cobalt chrome femoral stems manufactured using selective laser melting. *Materials and Design*, 60:177–183, 2014.
- [12] E Alva, T.H.C Tontowi, and Childs. Density prediction of crystalline powder sintered parts at various powder bed temperatures. *Rapid Prototyping Journal*, 7, 2001.
- [13] M. Vasquez, B. Haworth, and N. Hopkinson. In-process sintering region for laser sintered nylon-12. *Proc. IMechE*, 225, 2011.
- [14] L Lu, JYH Fuh, and YS Wong. *Laser Induced Materials and Processes for Rapid Prototyping*. Kluwer, 2001.
- [15] N Hopkinson, H Zarringhalam, and C Majewski. Degree of particle melt in nylon-12 selective laser sintered parts. *Rapid Prototyping Journal*, 15, 2009.
- [16] H. Zarringhalam. *Investigation into crystallinity and degree of particle melt in selective laser sintering*. PhD thesis, Loughborough University, 2007.
- [17] C.E Majewski, H Zarringhalam, and N. Hopkinson. Effects of degree of particle melt and crystallinity in sintered nylon-12 parts. *19th Annual International Solid Freeform Fabrication Symposium*, 19, 2008.
- [18] U Ajoku, N Hopkinson, N Saleh, R Hague, and P Erasenthrian. Investigating mechanical anisotropy and end-of-vector effects in laser-sintered nylon parts. *Journal of Engineering manufacture*, 10, 2006.

- [19] W. Cooke, R.A. Tomlinson, R. Burguete, and V. Daniel Johns. Anisotropy, homogeneity, and ageing in an sls polymer. *Rapid Prototyping Journal*, 17, 2011.
- [20] R. R. Martukanitz. Taking the next step in additive manufacturing. *Welding journal*, 93:40–44, 2014.
- [21] J.P Kruth, X Wang, L Laoui, and Froyen. Lasers and materials in laser sintering. *Assembly Automation*, 23:357–371, 2003.
- [22] 3D Systems. 3d systems, duraform pa and gf, materials for sls systems. *Website*, 2013. Accessed 2015.
- [23] EOS. Eos gmbh, product information eosint p/pa2200-pulver, manufacturer supplied materials data sheet. *Data Sheet*, 2005.
- [24] J.-P Kruth, G Levy, F. Klocke, and T.H.C Childs. Consolidation phenomena in laser and powder-bed based layered manufacturing. *Annals of the CIRP*, 56(2), 2007.
- [25] K. Senthilkumaran, P.M. Pandey, and P.V.M. Rao. Influence of building strategies on the accuracy of parts in selective laser sintering. *Materials and Design*, 30(8):2946–2954, 2009.
- [26] B Caulfield, P.E McHugh, and S Lohfeld. Dependence of mechanical properties of polyamide components on build parameters in the sls process. *Journal of Material Processing Technology*, 182, 2007.
- [27] C. Majewski and N. Hopkinson. Effect of section thickness and build orientation on tensile properties and material characteristics of laser sintered nylon-12 parts. *Rapid Prototyping Journal*, 17(3):176–180, 2011.
- [28] U. Ajoku, N. Hopkinson, and M. Caine. Experimental measurement and finite element modelling of the compressive properties of laser sintered nylon-12. *Materials Science and Engineering*, 428, 2006.
- [29] L.S Thomas, J. Timothy, Gornet, and S.U John. The effect of process conditions on mechanical properties of lasersintered nylon. *Rapid Prototyping Journal*, 17(6):418–423, 2011.
- [30] N Moes, T Dolbow, and T Belytscko. A finite element method for crack growth without remeshing. *Int J Numer Methods Engng*, 46:131–150, 1999.
- [31] M.J. Pais. Matlab extended finite element (mxfem) code v1.2,. <http://www.matthewpais.com/2Dcodes>, 2011.

- [32] N Petrinic, JLC Sosa, CR Siviour, and BCF Elliott. Improved predictive modelling of strain localisation and ductile fracture in a ti-6al-4v alloy subjected to impact loading. *Journal De Physique. IV : JP*, 134:147–155, 2006.
- [33] T. Belytschko, R. Gracie, and G. Ventura. A review of extended/generalized finite element methods for material modeling. *Modelling and Simulation in Materials Science and Engineering*, 17:24, 2009.
- [34] J.L. Curiel Sosa and N. Karapurath. Delamination modelling of glare using the extended finite element method. *Composites Science and Technology*, 72:788–791, 2012.
- [35] M.C. Serna Moreno, J.L. Curiel-Sosa, J. Navarro-Zafra, and J.J Martínez Vicente, J.L. and. López Cela. Crack propagation in a chopped glass-reinforced composite under biaxial testing by means of xfem. *Composite Structures*, 119:264–271, 2015.
- [36] J. Navarro-Zafra, J.L. Curiel-Sosa, and M.C. Serna Moreno. Three-dimensional static and dynamic analysis of a composite cruciform structure subjected to biaxial loading: a discontinuum approach. *Appl Compos Mats*, 10.1007/s10443-015-9453-4, 2015.
- [37] J Fish and T Belytschko. *A First Course in Finite Elements*. John Wiley and Sons Ltd, 2007.
- [38] JL Curiel Sosa, E de Souza Neto, and DRJ Owen. A combined implicit-explicit algorithm in time for non-linear finite element analysis. *Communications in Numerical Methods in Engineering*, 22:63–75, 2006.
- [39] JL Curiel-Sosa, OA Beg, and JM Liebana Murillo. Finite element analysis of structural instability using an implicit/explicit switching technique. *International Journal of Computational Methods in Engineering Science and Mechanics*, 14:452–464, 2013.
- [40] AJC Molina and JL Curiel-Sosa. A multiscale finite element technique for nonlinear multi-phase materials. *Finite Elements In Analysis And Design*, 94:64–80, 2015.
- [41] T. Belytschko and T Black. Elastic growth in finite elements with minimal remeshing. *International Journal for numerical Methods in engineering*, 45:601–620, 1999.
- [42] T. Belytschko, W.K. Liu, B. Moran, and K. Elkhodary. *Nonlinear Finite Element Methods for Continua and Structures*. Wiley, second edition, 2013.
- [43] R. De Borst, M.A. Crisfield, J.C. Remmers, and C.V. Verhoosel. *Nonlinear Finite Element Analysis of Solids and Structures*. Wiley, second edition, 2012.
- [44] J.M. Melenk and I. Babuska. The partition of unity finite element method: Basic theory and applications. *Seminar for Applied Mathematics*, 1996.

- [45] N Sukumar, D Chopp, N Moës, and T Belytschko. Modeling holes and inclusions by level sets in the extended finite-element method. *Computer Methods in Applied Mechanics and Engineering*, 190:6183–6200, 2001.
- [46] M.Y. Wang, X. Wang, and D. Guo. A level set method for structural topology optimization. *Computer Methods in Applied Mechanics and Engineering*, 192(1-2):227–246, 2003.
- [47] M. Stolarska, D.L. Chopp, Moës N., and T. Belytschko. Modelling crack growth by level sets in the extended finite element method. *International Journal for Numerical Methods in Engineering*, 51:943–960, 2001.
- [48] N. Moes, M. Cloirec, P. Cartraud, and J. Remacle. A computational approach to handle complex microstructure geometries. *Computer Methods in Applied Mechanics and Engineering*, 192:3163–3177, 2003.
- [49] M.J. Pais. Matlab extended finite element method (mxmfem) users guide. *Mechanical and Aerospace Engineering Department University of Florida*, April 2010.
- [50] N. Hopkinson, C.E. Majewski, and H. Zarringhalam. Quantifying the degree of particle melt in selective laser sintering. *CIRP Annals - Manufacturing Technology*, 58:197–200, 2009.

## Highlights

- Degree of particle melt (DPM) in SLS parts affect and control both crack initiation and propagation.
- Assessment of fracture behaviour to investigate what is triggering a microcrack in the first instance.
- It was found that un-melted particles proximity was the triggering effect in the onset of a microcrack.
- A microcrack started invariably between the two closest un-melted particles in all numerical tests performed considering different arrangements of un-melted particles.